Measurement 263 (2026) 119920

Contents lists available at ScienceDirect

Measurement

journal homepage: www.elsevier.com/locate/measurement

Design and experimental verification of an isolated voltage probe for the 2 kHz–30 MHz interval operating in live conditions☆

Andrea Mariscotti

Department of Electrical, Electronics and Telecommunication Engineering and Naval Architecture (DITEN),University of Genoa, Genoa, 16145, Italy

ARTICLE INFO

Keywords:
Conducted emissions
Current probe
Electromagnetic compatibility
Radio-frequency
Uncertainty
Voltage probe

ABSTRACT

The work discusses the different options for RF voltage measurement in LV grids (both AC and DC) used to evaluate distortion and conducted emissions over an extended frequency range (0.002 MHz to 30 MHz). Important characteristics are galvanic insulation, fundamental suppression and decent sensitivity, to guarantee safety and to allow the connection of sensitive measuring equipment. The design and experimental verification of a prototype based on a controlled-impedance branch, whose current is measured clamping an insulated RF probe on a number of turns, are reported. The results show that attenuation of only 24 dB is achievable, with a significant mains fundamental attenuation larger than 20000. The high-frequency behaviour was trimmed by adding ferrite beads to some selected turns achieving a flat frequency response within ±0.1 dB up to the −3 dB point at 31 MHz.

1. Introduction

The assessment of power quality and distortion in modern grids goes through a reliable and accurate measurement of voltage over the extended frequency range covering supraharmonics (SHs) and radio-frequency (RF) conducted phenomena, namely between 2 kHz and 30 MHz [1]. The measurement of voltage at a grid port is also useful for the characterization of the impedance of the grid and of the connected loads [2–4].

Modern grids undergo high-frequency (HF) distortion and instability phenomena, as caused by static power conversion systems, such as those employed for electric vehicle charging and photovoltaic energy production at the high end, and all electrical and electronic equipment in residential, office-like and industrial contexts [5,6]. Voltage distortion is also responsible for electric stress on grid components and loads, promoting various ageing mechanisms [7].

The measurement of such quantity is nowadays carried out using both time-domain and frequency-domain instrumentation for a range of exigencies, such as achieving lower background noise and frequency selectivity, ensuring the ability of spotting out modulation effects and evaluating statistical distributions, detecting transients, etc. In general all methods share four fundamental exigencies.

- The input voltage on the measuring channel needs to be scaled down to a few volts maximum, including the need of suppressing the fundamental component and major low-order harmonics ("fundamental suppression") to improve the dynamic range; fundamental attenuation was not perceived as necessary, as long as the use of frequency-domain equipment was almost compulsory as per CISPR standards, but has become quite relevant using time-domain data acquisition systems.
- Galvanic insulation is also necessary at least to break any ground loop and unwanted coupling, but also as one of the methods to ensure electrical safety of equipment and operator.
- Being the voltage probe connected to an electric grid exposed to overvoltage and surge phenomena, its behaviour and reliability need to be guaranteed both in steady and in transient conditions.
- The internal noise should be low to improve sensitivity, allowing the measurement of spectral components of reduced amplitude, where electromagnetic compatibility (EMC) limits of 1 mV to 2 mV (60 dBμV to 66 dBμV) are usually considered at frequencies above 150 kHz [6] or starting from as low as 10 kHz with much higher limits, (> 90 dBμV [8].

Commercially available voltage probes may fail in one or more of these aspects and this is briefly discussed as justification and motivation of the present study.

In addition, technical requirements for the effective measurement of conducted emissions of electrical equipment in LV grids may be formulated:

☆ This research is performed in the scope of the project "23IND06 Met4EVCS - Metrology for electric vehicle charging systems". The project has received funding from the European Partnership on Metrology, co-financed by the European Union's Horizon Europe Research and Innovation Programme and by the Participating States.

E-mail address: andrea.mariscotti@unige.it.

https://doi.org/10.1016/j.measurement.2025.119920
Received 1 July 2025; Received in revised form 19 October 2025; Accepted 28 November 2025
Available online 13 December 2025

- the frequency response (FR) should extend from 2 kHz (including thus the so called supraharmonics [7,9]) up to 30 MHz (as per various EMC standards [6,8]);
- FR flatness ensures usability without complex FR correction, with 1 dB or less for best sensors;
- low internal noise and sufficiently small attenuation are needed to ensure appropriate sensitivity to measure low-amplitude spectral components; considering an order of magnitude below typical limit values [6], the equivalent noise at the high-voltage side should not exceed 100 μV;
- the input impedance must be sufficiently large not to disturb and load the equipment and grid under measurement at high frequency with a typical minimum value of 1500 Ω [10].

Inductive voltage transformers do not have a satisfactory FR extended deep in the MHz range. They surely meet the galvanic insulation requirement, but would still need a blocking capacitor, not only to attenuate the fundamental, but also to avoid saturation in case of presence of a DC component. The added 560 nF capacitor in [3] seems to have this purpose, although not explicitly commented.

Resistive or capacitive (or a combination thereof) voltage dividers are robust and reliable devices, able to operate at high voltages, but lack galvanic insulation. They are an example of the broad category of the so called Low-Power Voltage Transformers [9], discussed and recently characterized for the SH range in the relevant standards of the IEC 61869 family [11]. The FR varies significantly between models, and may range from a few kHz [12] up to several MHz [13], of course at a price. Often they are the preferred technical solution for the insulated high-voltage probes mentioned below. Also in this case suppression of the fundamental is not readily available.

The CISPR V-probe [14] provides a loading impedance to the grid of 1500 Ω, a nominal attenuation of 30 dB and an output impedance of 50 Ω, without galvanic insulation. Decoupling of the fundamental is carried out by a series blocking capacitor, whose value depends on the allowed amount of homopolar leakage current. The CISPR 16-2-1 specifies a value larger than 5 nF, without upper limit. This design has the advantage of simplicity and low noise, but needs further fundamental attenuation and galvanic insulation.

Insulated high-voltage (IHV) probes are quite common in any laboratory and they are able to measure up to one or some kV, with large bandwidth extended up to tens of MHz, providing galvanic insulation. In general such probes have larger internal noise and an unfavourably large dynamic range, being able to operate at DC and mains fundamental frequency too. IHV probes do not have in general fundamental suppression, except for one of the models shown in Table 1, the Hioki mod. 9322 that has a selectable cut-off frequency at 1 kHz (but the amount of attenuation is not specified).

IHV probes may be decoupled by interposing a series capacitor that, thanks to the high input impedance (in excess of 1 MΩ), may have very small value. It may be also necessary to reduce this high input impedance to improve the tolerability to stray capacitance and to electric noise, while controlling line loading: their input terminal may be parallelled by a high-voltage resistor in the order of some kΩ or tens of kΩ.

The least noisy models may anyway be used for measurement of the RF grid voltage with all concurring incoherent noise sources forming a background in the order of 1 mVrms at best. This background noise level appears in the results reported in [15], where it is remarkable that the lower 2 kHz to 20 kHz frequency sub-interval is characterized by a larger background noise, in the order of 10 mVrms, as a consequence of high-order harmonics and some spectral leakage. A similar behaviour is confirmed by the spectra reported in [16], showcasing measured emissions of electric vehicle chargers.

IHV probes have overall good performance, except for the limited sensitivity (due to the combination of large internal noise and large attenuation) and significant uncertainty at HF (although the Hioki mod. 9322 was individually calibrated and reported with a 0.1% uncertainty up to 150 kHz [17]). The characteristics of some probes for a suitable voltage range are summarized in Table 1.

A different approach relies, instead, on the measurement of the current flowing through a circuit featuring a known impedance [23]. The circuit is designed around a series-connected RC branch (resistor and capacitor). The galvanic insulation is ensured by measuring the flowing current with a RF current probe, so removing any electric connection. RF current probes are transformer based, with multiple secondary turns around a ferrite core with a bore to place around the conductor under measurement [24], that represents the primary winding that in our case is made of multiple turns. The bandwidth is that of the current probe, except for the introduced lower cut-off frequency of the series RC branch. The resistor value is decided for the desired loading of the grid and the 1.5 kΩ of the CISPR probe represents a reference value. As a further advantage the high-pass nature of the RF current probe provides additional fundamental attenuation. Publications [3,23] remain to author's knowledge the only publication proposing this approach, showing through the years different performance in terms of frequency extension: 10 kHz to 500 kHz the former, 20 kHz – 10 MHz the latter. The present work represents an improvement in many aspects: the design is thoroughly discussed, including aspects of electrical safety and ratings for extensive use in LV grids; the improved frequency interval both in the LF range (down to 2 kHz) and in the HF range (covering up to 30 MHz); variability and uncertainty are evaluated together with extensive experimental verification.

The RC-buffered IHV probe is kept as a reference, having selected the Testec Si-9010 [21] for a matter of availability and thanks to its very low noise and in general good performance. The design and performance of the proposed RC-buffered RF current probe will be discussed then in the following. The voltage probes are both shown in Fig. 1 and identified as "probe A" and "probe B", respectively. It is underlined that the resistor R_2 is split in two halves (R_{21} and R_{22}) to control common-mode (CM) loops, as it was observed during the first tests using a single resistor.

The application requirements as introduced above are discussed and quantified in Section 2, while discussing and justifying design choices. The design equations are formulated, showing the process for the optimization of the probe parameters (Section 3), further refining the design during the discussion of the results. The results of the experimental characterization of some prototypes, including the evaluation of the uncertainty, are reported in Section 4.

2. Application requirements and design development

2.1. Electrical insulation and electrical safety

For the electrical safety ratings the IEC 61010-1 [25] provides reference for the grid nominal voltages the measuring instrument is connected to and the expected overvoltage levels. The Annex F of the IEC 61010-1 indicates routine tests (that can thus be repeated at will without risk of deteriorating the insulation), consisting of an AC or DC test voltage $V_{t,ins}$ raised to the prescribed value in 5 s and then held for at least 2 s. The $V_{t,ins}$ is to be determined as the combination of the mains nominal line-to-neutral voltage V_n and the overvoltage category (OV-Cat), as shown in Table 2. To note that for applicability to DC grids, V_n indicates then the positive-to-negative voltage; DC supply is less critical than AC in terms of partial discharge phenomena, occurring mostly at zero crossings, and for exposure to lightning-induced phenomena, being usually of small extension and buffered from medium voltage distribution. In addition, the input capacitors have a much higher rating at DC and will block any leakage.

The OV-Cat is to be determined depending on the level of exposure to lightning phenomena and switching overvoltages of the line the instrument is connected to, as clarified in the Annex K of the standard. The OV-Cat ranges from I (for protected sockets within buildings) to

Table 1
Characteristics of selected high-voltage insulated probes.

Description	Input range	Atten.	Bandwidth	Internal noise
Hameg HZ115 [18]	1400 V	1000:1	20 MHz	2 mVrms
Tektronix THDP0100 [19]	600 V	100:1	100 MHz	175 mVrms
Tektronix TMDP0200 [19]	75 V	25:1	100 MHz	25 mVrms
Testec SI-9002 [20]	1400 V	200:1	25 MHz	14 mVrms
Testec SI-9010 [21]	700 V	100:1	70 MHz	0.9 mVrms
Hioki 9322 [22]	2000 V	1000:1	10 MHz	—

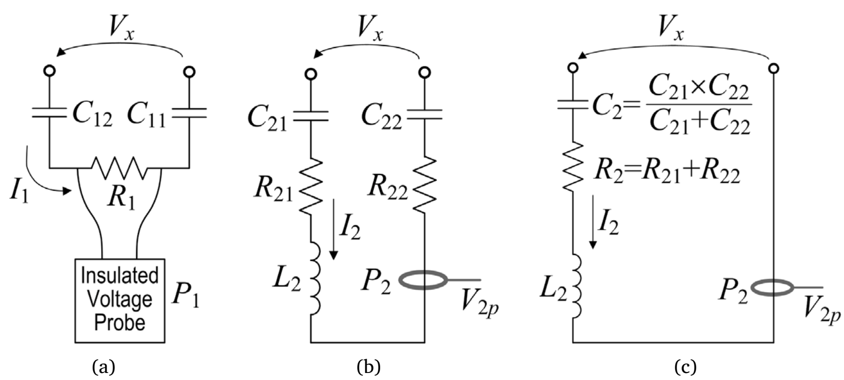

Fig. 1. Schematics of the discussed voltage probes: **(a)** (Probe A) RC-buffered IHV probe (indicated as "P_1"); **(b)** (Probe B) current probe "P_2", buffered by a symmetric RC circuit for CM rejection; **(c)** simplified schematic of (b) used for some calculations.

Table 2
Insulation routine test levels $V_{t,ins}$ for DC, AC and 1.2/50 μs impulsive tests.

Nom. L-N voltage V_n	OV-Cat II			OV-Cat III			OV-Cat IV		
AC rms or DC (V)	AC (Vrms)	DC (V)	Impulse (Vp)	AC (Vrms)	DC (V)	Impulse (Vp)	AC (Vrms)	DC (V)	Impulse (Vp)
$150 < V_n \leq 300$	1400	2000	2000	2200	3100	3100	3300	4700	4700
$300 < V_n \leq 600$	2200	3100	3100	3300	4700	4700	4300	6000	6000

IV (for installation near the point of common coupling, within main switchboards with high exposure, or if a high degree of reliability and availability is desired).

The rated nominal voltage for the probe must be taken as the maximum AC or DC voltage of a low-voltage (LV) grid, namely 1 kV for AC grids and 1.5 kV for DC grids. It is worth remembering that the highest nominal voltage of LV AC grids is 690 Vrms and is quite uncommon; conversely, DC grids are usually operated at 800 V, or lower, for photovoltaic systems and charging stations, with occasional implementations at 1 kV to 1.2 kV.

The voltage withstanding capability may be achieved by galvanic insulation (e.g. by means of a transformer or optocoupler establishing a galvanic barrier with sufficient dielectric strength), or, alternatively, a low leakage conductive path may be established (so that although the operator is coupled to the source voltage, the flowing current is below accepted safety thresholds). For current at the mains frequency the IEC 61010-1 [25] establishes a $I_{\text{lim,N}} = 0.5$ mArms limit in normal conditions and a $I_{\text{lim,F}} = 3.5$ mArms limit in fault conditions (i.e. when the low-leakage barrier is a mitigation in addition to a primary barrier, such as the galvanic one implemented by the current probe, that may fail).

Such a low-leakage barrier should be implemented with high-integrity capacitors, namely "safety capacitors" of the "Y" type, rated for the nominal grid voltage. In a 400 Vrms supply system, the corresponding capacitance limit under 230 Vrms of phase-to-ground voltage is 5.7 nF at 60 Hz for the 0.5 mArms limit, or 40 nF for the higher 3.5 mArms limit. Going to a 690 Vrms supply system with 400 Vrms of phase-to-ground voltage, the two capacitance limit values are reduced to 3.3 nF and 23.3 nF, respectively. This considering the capacitive reactance alone, much larger than the series resistive components at the mains frequency.

2.2. Transient overvoltage protection

Overvoltages may occur as the result of switching of reactive loads, energization/de-energization of lines, or lightning phenomena. In general, lightning is taken as reference using the fast test waveform (1.2/50 μs, whose waveform expression is fully reported in the EN 61000-4-5, Annex E [26]).

At the fast rising edge of 1.2 μs (corresponding to a frequency of about 300 kHz), the capacitive reactance is 53 Ω, so an initial large voltage across R_2 is expected; however, the power dissipation considering the low repetition rate of the applied surge is well within the limits, with only 75 mJ of energy released by a single pulse for an assumed $R_2 = 1.5$ kΩ and choosing the worst-case 4 kV surge test. This is well in the limits of any 0805 or 1206 SMD resistor, considering that there are 6 series connected items. The resulting peak voltage is then 600 V for each of them, so only 3 times higher than the normal working voltage.

The tolerability to transient voltages for non-repetitive pulses (surge test pulses are typically separated by one minute) is specified in the EN 140401-801 [27], Fig. 6, showing about 28 W for the package 1206 and pulse durations below 100 μs, as in the present case. The power dissipated during the transient is 378.1 W for a 4 kV pulse and 94.5 W for a 2 kV pulse. The latter corresponds to 15 W per resistor, so within the specification; for levels higher than 2 kV it is mandatory to protect the resistor R_2 with a spark gap, e.g. with a 1.8 kV threshold, thus covering also the 2 kV pulse for increased safety margin.

The voltage and current waveforms for the worst-case 4 kV surge test waveform are shown in Fig. 2.

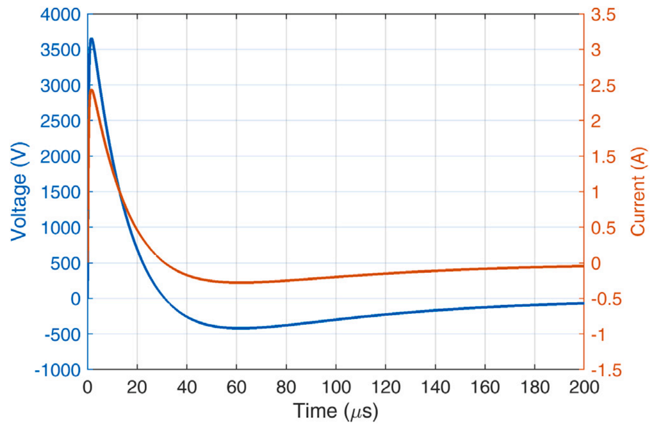

Fig. 2. Voltage and current waveforms for a 4 kV 1.2/50 μs surge test on the input RC branch of probe B.

2.3. *Attenuation of fundamental and low-order harmonics*

Attenuation of the fundamental and low-order harmonics is very important, in order to reduce dissipation on internal components on the one hand, and on the other hand to provide a suitably reduced dynamic range for the connected instrumentation. A high-pass circuit is implemented using the RC branch amounting to 30 dB of attenuation, if a 50 Hz fundamental and a cut-off frequency at 2 kHz are considered. A 690 Vrms voltage plus its harmonics would translate into more than 32 Vpk after attenuation. Considering the electrical insulation test level up to 3 kVrms, this translates into a temporary 100 Vrms voltage after the RC when testing.

An additional pole may be introduced by exploiting the high-pass behaviour of the current probe with its own cut-off frequency, usually in the tens or at a hundred kHz, providing thus another 30 dB of attenuation of the fundamental at the minimum operating frequency of 2 kHz.

2.4. *Frequency response*

The chosen frequency interval is the most challenging nowadays, comprehensively covering various frequency ranges that may fall within or at the margins of applicable standards. The 2 kHz to 150 kHz SH range is not yet fully covered by applicable EMC standards, where the minimum frequency in many cases is reported as 9 kHz or 10 kHz in an EMC perspective [6,8,28]. The 2 kHz to 9 kHz is instead included in the IEC 61000-4-30 [29]. Traditionally many EMC standards focus on the 0.15 MHz to 30 MHz range for emissions. The CISPR 16-1-2 [10] at its sec. 5.1 then indicates initially a frequency interval as large as 30 Hz to 1000 MHz, but when narrowing down to desired performance and specifications, the frequency interval is reduced to 0.1 MHz to 100 MHz, necessitating specific probes to cover higher frequencies up to 1000 MHz. For voltage probes the CISPR 16-1-2 at its sec. 5.2 reports the already mentioned “CISPR 1500 Ω probe” specified over the 9 kHz – 30 MHz frequency range, with a 1 dB accuracy limit for the influence of any added protecting device (if not included in the calibration), from which we get an indication of the overall accuracy acceptable performance.

2.5. *Sensitivity and internal noise*

The sensitivity of the proposed scheme is based on the transfer impedance (Z_t) of the RF current probe that is in the order of some Ω for many models. The input resistance reduces the signal that is then increased proportionally by the number of turns, in the range of $N = 12 \ldots 15$. The resulting sensitivity is thus comparable with a 50 Ω resistor, having assumed Z_t of some Ω (the selected RF probe has a maximum Z_t value of nearly 8 Ω).

The internal noise is minimum, being prevalently that at the output of the RF current probe itself, featuring a 50 Ω output impedance, thus comparable to that of the CISPR probe.

3. Detailed design and prototype

Both probes (Probe A considered as reference and the proposed Probe B) adopt mains decoupling by series capacitors, that helps also to ensure voltage withstanding capability. The values of the capacitors are selected to prevent mains current leakage and to trim the low cut-off frequency.

3.1. *Probe A: modified insulated voltage probe*

Since the voltage probe alone provides galvanic insulation, the added RC branch is to be sized for $I_{\mathrm{lim,F}}$. This leads to a total maximum capacitance of 23.5 nF (two series 47 nF capacitors C_1 and C_2 on each phase or phase and ground) and a series resistor R_1 that provides the correct cut-off frequency and loading of the grid. For cut-off at 2 kHz the resulting value is 3.3 kΩ. If it is deemed too low, the capacitors may be reduced to 22 nF, resulting in 11 nF and the resistor increased to 7.4 kΩ to keep the lowest cut-off frequency. In general, considering 1500 Ω an adequate loading in line with the CISPR V-probe, a slightly higher cut-off frequency may be accepted. Capacitors of 22 nF may be preferred not only for a matter of lower leakage current, but also because they are the largest value usually available as Y safety capacitors for the desired voltage range (500 Vrms).

The downstream probe is selected considering existing commercial products, some of which are reported in Table 1. For a matter of availability and preferring its low internal noise, the selected probe for the tests is the Testec mod. 9010.

3.2. *Probe B: RC branch with RF current probe*

There are many reasons for choosing to measure the grid voltage by means of a flowing current through a known impedance branch: RF current probes have in general good performance and there is a wide range of choice; galvanic insulation is granted by the working principle of the probe and the RC values may be more freely selected; due to the current probe high-pass behaviour, overall attenuation of mains and harmonic components is improved.

As already discussed for probe A, the total series capacitor may be selected as high as 23.5 nF, as done for the prototype due to availability of 47 nF capacitors to connect in series. The already mentioned $R_2 = 7.4$ kΩ resistor would provide the desired 2 kHz cut-off frequency, resulting, however, in excessive attenuation. So the 1.5 kΩ value is considered for comparison with the probe A and the CISPR probe, increasing the cut-off frequency; the value is evenly split into $R_{21} = R_{22} = 750$ Ω.

One may object that the I_2 current reduction using a large overall R_2 value can be compensated by increasing the number of turns N_2 through the probe, at the expense, however, of increased inductive reactance and worsening of the HF response.

Although compensation by increasing N_2 seems easy to apply whatever the R_2 value, the so created parasitic inductance L_2 increases with N_2^2 with higher chances of self-resonance. N_2 must be thus traded off with R_2, keeping the total winding reactance X_{L2} smaller than or similar to R_2 at the largest frequency (30 MHz). A bottom limit to reducing R_2 is keeping the line loading acceptable, so that a 1.5 kΩ limit value may be chosen, as in the original CISPR probe.

With an unknown voltage to measure V_x, the resulting current is $I_2 = V_x / Z_2$ ($Z_2 = R_2 + jX_{L2}$ being the total impedance of the branch), to multiply then by N_2 and the transfer impedance of the current probe

Table 3
Analysed parameters configurations for probe B FR.

case	$C_{21}//C_{22}$ (pF)	R_2 (Ω)	N_2
I	11	7.5k	15
II	5.5	7.5k	15
III	11	1.5k	15
IV	11	1.5k	10
V	11	1.5k	12

$Z_{t,p2}$, giving the output voltage V_{p2} (quantities are annotated in the schematic of Fig. 1).

$$V_{p2} = V_x \frac{Z_{t,p2}\, N_2}{Z_2} \tag{1}$$

Some curves of overall sensitivity $S_s = V_x/V_{p2}$ are plotted in Fig. 3, as resulting from the range of values of the discussed parameters. The considered combinations are identified as case I through V, as described in Table 3.

Since the selected RF current probe (TekBox mod. TBCP1-200 [30]) is not characterized for frequencies below a few kHz, transfer impedance values were just estimated by extrapolation of the available values, and this may be a source of error for the simulation of the behaviour at the lowest frequencies (where the interest, however, is focused only on fundamental attenuation).

The centre-band gains (taking the maximum values) are $G_I = G_{II} = 0.0159$ (i.e. −35.98 dB), $G_{III} = 0.0794$ (i.e. −22.0 dB), $G_{IV} = 0.0548$ (i.e. −25.23 dB) and $G_V = 0.0635$ (i.e. −23.94 dB). However, it may be observed how the highest curve (violet) suffers from the effect of the parasitic inductance by effect also of the lower R_2 value; conversely, the 'case IV' curve (green) has a sufficient flatness and the gain is only 35% less. Since there is some approximation in the calculation of the overall inductance, having used the formula for the perfectly compact and coupled solenoids, more flatness is expected from the real winding. In addition, two factors influence the accuracy of the calculation of the primary winding inductance: the magnetic permeability of the probe material reduces with frequency, so that a high-frequency value was selected; the use of coupling between non-adjacent turns by means of ferrite beads reduces the overall inductance, as it will be discussed in the experimental Section 4. The intermediate case V was added to ease the comparison between simulations and measurements.

We may conclude that the target attenuation value at around −20 dB is achieved with the largest numbers of turns in the order of $N_2 = 14 - 15$. In this case the centre-band gain is −22.6 dB and −22.1 dB, respectively. $N_2 = 14$ is preferred to achieve the desired 30 MHz bandwidth, as it will be shown in Section 4.

The attenuation of the fundamental (comparing with the centre-band gain) is 109.8 dB or 309k for the three cases III, IV and V; case I is the worst one, and case II is 102.7 dB or about 136k. Considering the lowest working frequency of 2 kHz the fundamental attenuation with respect to the lowest useful frequency reduces then to 63.3 dB for cases II, III, IV and V, being all in the constant slope roll-off region. The estimate of the fundamental attenuation is approximate, as it depends on the TBCP1-200 response at such low frequency, that is not documented and was estimated by extrapolation with a pure 20 dB/decade slope.

The overall roll-off at LF is determined by the combined action of the series RC branch and the desensitization of the RF current probe, resulting in almost a 40 dB/decade slope (the attenuation between 1 kHz and 10 kHz is approximately 70, so 36.9 dB).

To ease the comparison with the experimentally verified cases, simulations are repeated for cases III, IV and V using an equivalent capacitance of 23.5 nF (using $C_{21} = C_{22} = 47$ nF) and the results are shown in Fig. 4. Centre-band gains remain the same and the 50 Hz fundamental attenuation reduces to about 103 dB or 145k for all three cases III, IV and V. It is observed that the reduction is about a factor 2, corresponding to the capacitance increase, as expected.

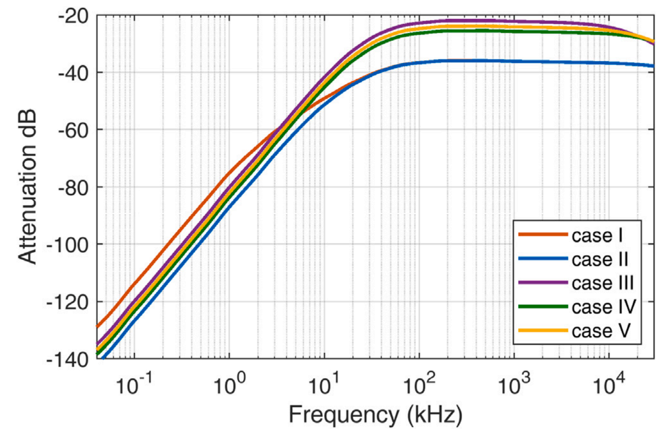

Fig. 3. Frequency response including the RC high-pass behaviour (with total capacitance $C_2 = 11$ nF) and the current probe transfer impedance: cases and parameters as per Table 3.

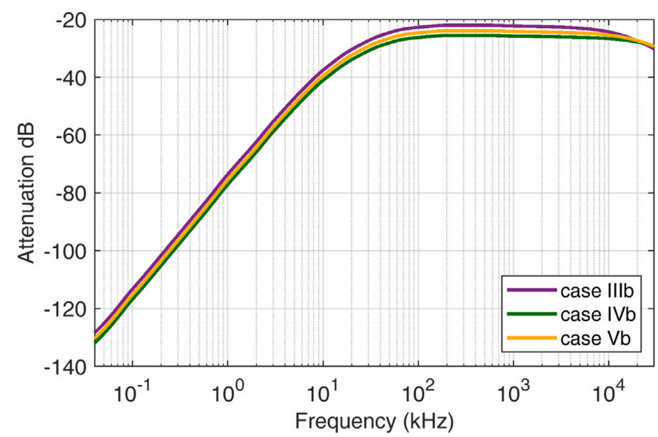

Fig. 4. Frequency response including the RC high-pass behaviour (with total capacitance $C_2 = 23.5$ nF instead of 11 nF) and the current probe transfer impedance: cases and other parameters as per Table 3.

R_{21} and R_{22} are built with multiple series-connected SMD resistors with an individual value selected to limit self heating. With the previously calculated maximum leakage mains current of 3.3 mArms, dissipation would be only 2.9 mW on a 270 Ω resistor. The series connection of 6 resistors (3 each side, for R_{21} and R_{22}, respectively) would provide $R_2 = 1620$ Ω. Harmonic components see a reduced capacitive reactance and are relevant for dissipation, so that they are included in the estimate. A worst-case 60 Hz mains frequency with 400 Vrms to ground and large harmonic distortion is considered and results are shown in Table 4. The resulting dissipation for the 1.2 kΩ to 3.6 kΩ range confirms an almost linear relationship and a low dissipation per device, about 22 mW maximum for each 270 Ω resistor (so 10% of the rating of a 1206 package).

As it will be shown experimentally in Section 4, the introduced winding around the current probe must achieve a trade-off between gain (proportional to the number of turns N_2) and self resonance (occurring between 15 MHz and 30 MHz, lower when N_2 is larger). After attempts to optimize the stray capacitance by separating the turns (that, however, requires a complicate and unfeasible arrangement of the winding), ferrite beads were introduced in the winding coupling some non-adjacent turns with a double objective: increase distributed resistance to dampen resonances and provide mutual coupling between non-adjacent turns, realizing a sort of cross-coupled filter.

The used beads are Richco mod. RT-80-60-50 [31], whose impedance curve is shown in Fig. 5. Looking where the linear region

Table 4
Dissipation estimation for distorted voltage for Probe B.

V_1 (V)	V_5 %	V_7 %	V_9 %	V_{11} %	V_{13} %	V_{17} %	V_{19} %	R_2 (kΩ)	P (mW)
400	20	14	11	10	10	5	5	3.6	302
400	20	14	11	10	10	5	5	1.8	163
400	20	14	11	10	10	5	5	1.2	110

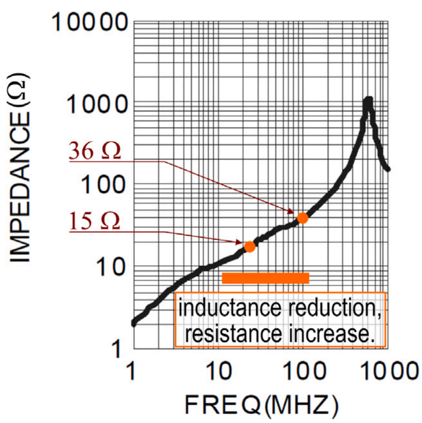

Fig. 5. Impedance curve of the selected ferrite bead Richco RT-80-60-50 [31] with annotations, showing the two frequency points where the manufacturer declares the bead impedance value.

ends, at 7 MHz the impedance value is slightly smaller than 10 Ω, that corresponds to about 220 nH, if assumed purely inductive. At the first declared value of 15 Ω at 25 MHz, the inductance has already decreased (under a purely inductive assumption it would be 95 nH) and the resistive components is increasing, although the manufacturer does not provide any information. This latter value is slightly larger than the inductance of one turn (estimated at about 60 nH to 70 nH for frequencies around the resonance). Such beads were identified as a compromise between their small dimension and their good electrical behaviour verified experimentally.

An equivalent circuit was created allowing the qualitative study of the achieved electrical behaviour, as shown in Fig. 6. The reason for saying “qualitative” resides in the fact that such circuit is approximate, not including magnetic and capacitive coupling between non-adjacent turns, that is particularly relevant as the winding is non planar. The reason is that there is a significant difference in the two curvature radii of the internal and external lateral surfaces of the probe. A formal approach to the derivation of the equations of a lumped circuit with cross-coupled terms is presented in [32], where both inductive (as in the present case) and capacitive cross-coupling terms are considered. The winding total length l_w is calculated as $N_2 \times l_t$, where l_t is the length of one turn, provided by the geometry of the current probe and equal to 116 mm; for N_2 ranging between 9 and 14, $l_w = 1.04$ m to 1.63 m, which is still electrically short with respect to the maximum useful frequency of 30 MHz. The equivalent circuit is a lumped parameter scheme.

The determination of the turn inductance needs the quantification of the AL parameter, using the same approach in [33]. The TBCP1-200 current probe exploits a high-permeability magnetic material with nominal $\mu_r \approx 4200$. The equivalent number of turns at the secondary N_{22} may be estimated by means of the expression R_{eq}/Z_t, where R_{eq} is the parallel of the internal and externally connected 50 Ω resistors, and Z_t is the nominal transfer impedance value in the centre-band region (see Fig. 7). The resulting number of turns is equal to $25/7.71 \approx 3$. The resulting secondary inductance is calculated considering the zero frequency f_1 of the Z_t frequency response of the TBCP1-200, that occurs slightly above 40 kHz, resulting in $L_{22} = R_{eq}/(2\pi f_1) = 99$ µH. The resulting $AL = L_{22}/N_{22}^2 = 9.5$ µH/turn^2.

With high-permeability cores the HF interval occurs where μ_r is no longer at its nominal initial value: in our case, assuming a behaviour similar to the N30 material (that has exactly a value of 4200 of initial permeability and has graceful degradation of permeability), μ_r reaches a value of about 100 around 10 MHz to 15 MHz, and AL, as a consequence, reduces to about 200 nH/turn^2. At 30 MHz it is expected that AL reduces by another factor of 2, minimum. This matches the initial guess having assumed a high-frequency low-permeability material.

The effect of the achieved mutual magnetic coupling between non-adjacent turns is that of reducing the total winding inductance by partially shunting some turns. The previously estimated bead inductance values indicate that the large LF value (about 3 times the turn inductance) keeps the shunting effect negligible, until the bead inductance reduces with frequency increasing the shunting effect. This is accompanied by an increase of resistance, that dampens the resonance experimentally found around 20 MHz to 25 MHz, as it will be discussed later. The increase of resistance is based on the following observation (looking at the bead impedance curve in Fig. 5 provided by the manufacturer). If inductance begins reducing at about 7 MHz, and should keep reducing with increasing frequency as it occurs for all common ferrite materials, then the slightly upward curve between 20 MHz and 50 MHz may be justified only by an increase of resistance. The manufacturer does not provide more detailed information on this. This behaviour is then verified experimentally by observing the beneficial damping of resonance effects.

The introduced beads were modelled as mutual inductance M between two different point belonging to the two involved turns (in the example $M_{2,N-1}$) and an increase of the respective longitudinal resistance values (in the example R_2 and R_{N-1}). Second-order coupling terms (such as coupling between non-adjacent turns and proximity effect between turns) are surely non-negligible and do not allow a reliable FR simulation, relying then on careful experimental assessment.

4. Experimental verification and estimate of uncertainty

Prototypes of both probes were built as shown in Fig. 8, together with the measurement setup and the arrangement of the calibration.

4.1. Measured performance

This section focuses mainly on the verification of the fundamental attenuation and frequency response.

4.1.1. Fundamental attenuation

The fundamental attenuation corresponds to the ratio between the applied 50 Hz input voltage and the resulting output voltage. Since values four to six orders of magnitude are expected, the test setup is arranged as follows: multimeters (Agilent model 34401A [34]) are used for both the measurement of the input and output voltages, the former set to a hundred Vrms, the latter measurable with sufficient accuracy in the mV range. A check was done of the existing noise including e.g. internal noise and interference from the power distribution, and it was found less than 2 µV. This value is perfectly compatible with the supposed internal noise source of about 50 Ω and an equivalent 34401A bandwidth of one or few MHz (larger than the 300 kHz one with guaranteed accuracy). This confirms the significant improvement compared to the output noise of IHV probes.

The tested version of probe B is the one with 9 turns and resulted in 0.53 mVrms, having applied 102.4 Vrms, providing a ratio of 5.17×10^{-6},

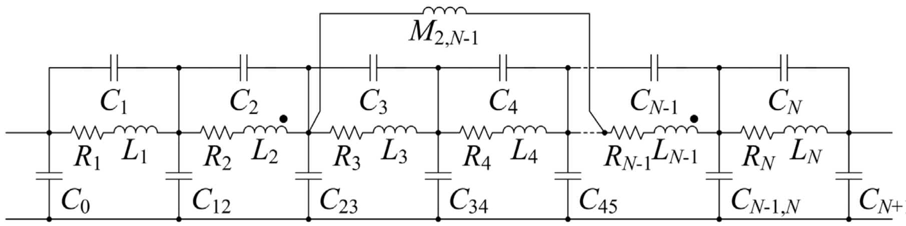

Fig. 6. Equivalent circuit of the winding with inserted ferrite beads between non-adjacent turns (a ferrite is shown as example between turns 2 and $N-1$, with a mutual coupling term and larger longitudinal resistance terms R_2 and $R_{(N-1)}$).

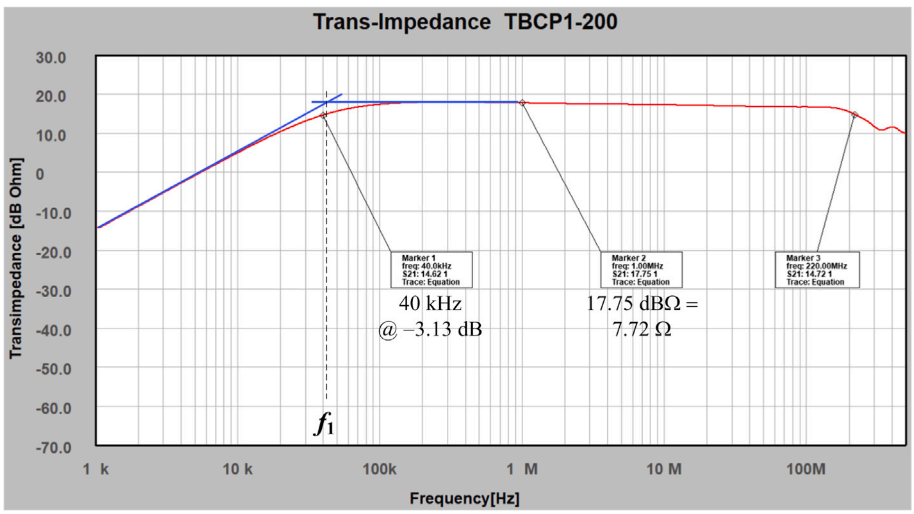

Fig. 7. Annotated transfer impedance Z_t curve of the TBCP1-200 current probe [30] for the estimation of the relevant equivalent circuit parameters (relevant text has been magnified with annotations).

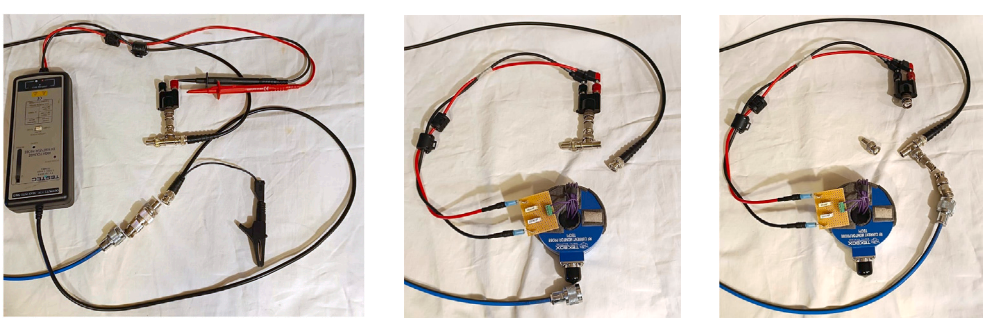

(a) (b) (c)

Fig. 8. Pictures of the probe prototypes ((a) probe A and (b) probe B) and (c) calibration arrangement. To note that the RC circuit located at the red/black adapter for probe A does not appear in the photo.

or -105.7 dB. Considering the centre-band gain of about -27 dB and that the output will be connected to a 50 Ω matched signal input (for which a reduction of 6 dB must be added), the overall suppression of the fundamental is in the order of $20000 : 1$. The suppression of low-order harmonics was evaluated overall by measuring the attenuation at 700 Hz, equal to 1.18×10^{-4}, providing an overall suppression of low-order harmonics in the order of $2000 : 1$. This prevents deterioration of the dynamic range due to out-of-scale events of low-frequency components, that result all confined well within 50 mVpk. The first “useful” frequency at 2 kHz, three times higher than the reference 700 Hz frequency, is characterized by an almost 20 dB reduced attenuation, setting a clear minimum separation of low- and high-order harmonics. This 20 dB factor is due to the 40 dB/decade slope characterizing that frequency interval projected onto the ratio of about 3 between 2 kHz and 700 Hz.

4.1.2. Frequency response

The FR $H(f)$ is determined by a swept sine test using a vector network analyser (VNA). The VNA is an Anritsu model MS2036C [35] with a minimum frequency of 5 kHz; to complete the frequency range down to about 1 kHz a few points were added using an RF signal generator and a spectrum analyser, and included in the data vector using interpolation for plotting. A manual measurement then with a multimeter was carried out for verification taking some readings up to

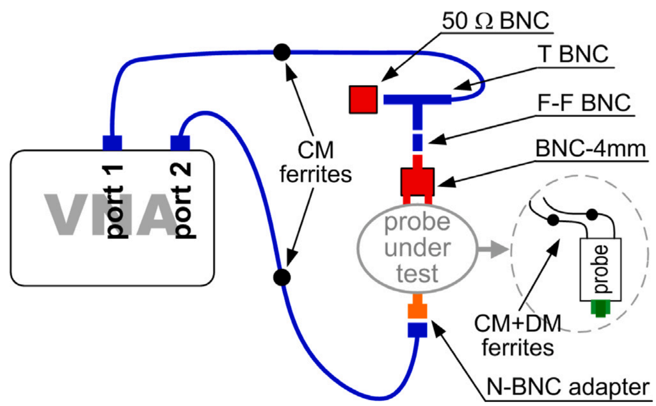

Fig. 9. Frequency response measurement setup with VNA Through calibrated part (in blue), additional elements (in red) and adapter used only for probe A (in orange). Black dots indicate ferrites (CM on the blue coaxial cables and differential mode (DM) on the probe wires).

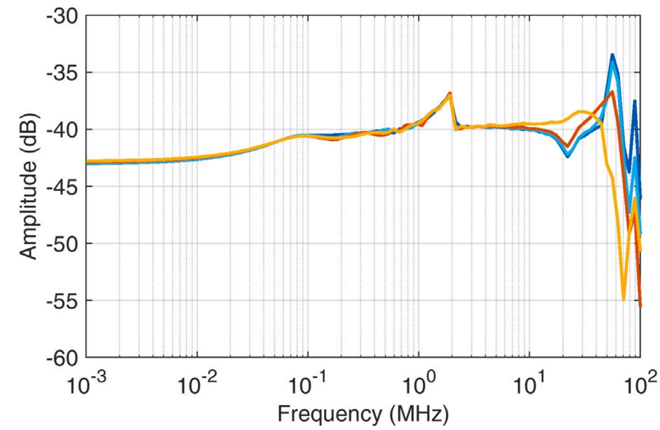

Fig. 10. Frequency response for probe A: dark and light blue curves refer to the case with no ferrites and different orientation of input wires (always twisted together); orange and yellow curves showing effect of ferrites with 1 and 2 turns, respectively.

30 kHz. The VNA in the following is used in "high-power mode", so at 3 dB of injected signal.

An amplitude-only S_{21} measurement was carried out using the setup described in Fig. 9. The S_{21} forward transmission parameter corresponds to the fraction of port 1 signal (V_1) that is transmitted to port 2 (V_2), which represent the voltage applied to the probe input and that appearing at the output of the RF probe, respectively. Reflected waves due to impedance mismatch that represent a source of error are discussed later in Section 4.2.3.

$$S_{21} = \frac{V_2}{V_1} \tag{2}$$

The S_{21} values are then plotted in the following as amplitude-only frequency response curves.

In the figure it is possible to observe a blue part of the schematic that is the one compensated by the "Through" calibration (transmission only). The measuring loop of cables and adapters was kept short (0.5 m of high-quality semi-rigid RF cable on port 2 and 0.6 m of flexible RG58 cable on port 1), in order to minimize the effect of reflections due to residual mismatch. When, after the Through calibration, the loop is broken and the probe is inserted in the middle, the following adjustments were made (marked in red or orange in Fig. 9, shown later in Section 4.2.3):

- a 50 Ω termination was added on channel 1 to replace the termination provided by port 2 during the calibration; the difference between the two 50 Ω values is negligible, in particular for the frequency range of interest (up to 30 MHz and measured up to 100 MHz);
- one N-BNC adapter was removed (used to create the Through between the N terminated and the BNC terminated lines; the adapter is kept instead to test probe A, that terminates in a BNC connector;
- one BNC to 4 mm banana sockets was included, approximately of the same physical length of the removed adapter.

The 50 Ω load puts the injecting line in matched conditions and the probe with its input impedance is derived in parallel next to the added matched load. Its effect in electric parallel is minimal: the nominal 1500 Ω resistive input impedance effect on the 50 Ω results in 48.4 Ω, with a reflection coefficient of 1.6%. The wavelength at the maximum frequency in the RG58 cable with velocity factor of 0.66 is 6.6 m, so that the 0.6 m line length results in a less than $\lambda/10$ condition at the maximum frequency of interest.

First tests were performed on the probe A using the commercial Testec insulated probe and the results are shown in Fig. 10. It is apparent that resonances are present although CM and DM ferrites are located on the connecting wires. The blue curves (dark and light) refer to the same setup with only one CM ferrite when changing the path of the incoming probe wires and no significant change is visible up to about 70 MHz, although a sharp resonance at 55 MHz is easily visible. This FR resonance appears despite the significant CM impedance of the coupling wires. It was thus postulated that its origin must be sought in the DM circuit, for which specific ferrites were added. The dark orange curve results from including one DM ferrite on each wire, improving when bring the wire turns to two (dark yellow curve). The ferrites are Richco mod. RRC-16-8-16 [36] featuring 150 Ω at 30 MHz. Such ferrites cure the problem related to the input stray capacitance, shunting the signal and causing resonances, by increasing both the CM and DM impedance at HF with a significantly large resistive component. As evident, they also suppress the HF dampened resonance at 70 MHz to 80 MHz.

Tests were carried out on probe B with a variable number of turns N equal to 14, 12 and 9. As expected the centre-band gain is proportional to N, but the behaviour at HF, instead, is much less intuitive. What is determinant is the effect of the applied compensation by means of ferrite beads on some of the turns with a double objective: increase distributed resistance to dampen resonances that may occur and provide mutual coupling between non-adjacent turns, realizing a sort of cross-coupled filter. The latter has been tested experimentally, but no formal theoretical approach has been attempted. The used beads are Richco mod. RT-80-60-50 [31], featuring 15 Ω at 25 MHz, that corresponds to 89 nH if assumed purely inductive. This is roughly the same amount of inductance of one turn and it is believed to allow fine tuning, although smaller values may be tried too. It is noted that EMI suppression beads that are commercially available are tailored for the hundreds of MHz and GHz ranges, so that it is difficult to find small ferrite beads with a significant resistive components already at 30 MHz, as in the present case. It must be underlined that turns in the coil are distributed over the transversal circumference, so coupling is achieved with limited accuracy of half a turn, depending if the bead is placed on the top or bottom of the current probe flat surfaces.

Fig. 11 shows the effect of the already used Richco clamp-on ferrites (RRC type [36]) located on the input wires, having verified the FR by reversing the connection of the plus and minus polarity. The two blue curves refer to the case of using one Richco on each wire with just one turn: reversing the polarity does not change the FR and the circuit is symmetric and balanced well up to 100 MHz. Conversely the two orange curves taken without such ferrites show a difference of some dB starting

Table 5
Tested cases of ferrite beads arrangements for the $N = 14$ turns coil.

Curve no.	1	2	3	4	5	6	7	8	9	10	11	12	13	14
45	N	N	N	N	Y1	Y2	N	N	Y2	Y1	N	N	N	N
50	N	N	N	Y1	Y2	N	N	N	N	Y2	Y1	N	N	N
51	N	N	Y1	Y2	Y2	N	N	N	N	Y2	Y2	Y1	N	N
52	N	N	N	Y2	Y2	N	N	N	N	Y2	Y2	N	N	N
53	N	N	N	N	Y2	N	N	N	N	Y2	N	N	N	N

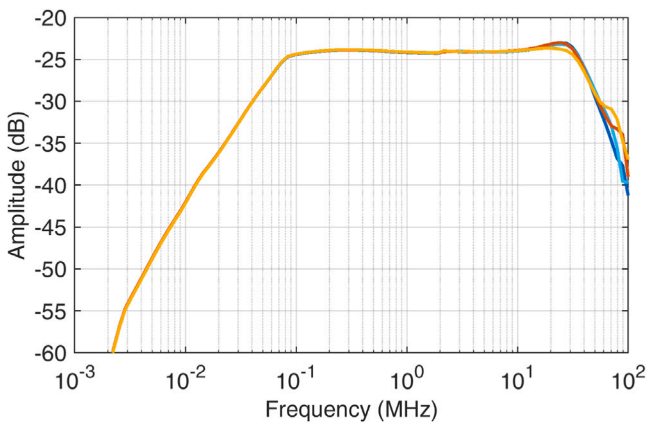

Fig. 11. Frequency response for $N = 14$ turns with ferrites (blue curves) and no ferrites (orange curves) on the input cables; dark and light colour refer to the two different polarities of the input wires.

from about 15 MHz. All tests are from now on done with the probe B equipped with these two Richco ferrites on the input wires.

The previous statement regarding the positive effect of ferrite beads on selected non-adjacent coil turns is demonstrated in Fig. 12, where the magenta curve refers to the case with no ferrite beads and the black curve is obtained having applied two beads each clamping on turns 5–10 and 6–9 of a 14-turn coil (curve “45” as per the VNA numbering). This configuration and the others of Fig. 13 are summarized in Table 5.

By comparing the curves of Fig. 13, it appears that curve 50 provides the best results in terms of bandwidth (the largest, right 31 MHz at −3 dB) and flatness of ±0.1 dB around −24 dB. Giving up some flatness, light and dark blue curves in Fig. 11 obtained without ferrite beads within the winding provide 44 MHz of −3 dB frequency extension at the price of a ±0.6 dB variation of the frequency response around −23.6 dB. The configuration of curve 50 is the preferred one and will be selected for the final realization after some additional verifications of stability with respect to repeated use and geometry of connection.

A demonstration that reducing the number of turns might not lead immediately to a more favourable situation in terms of resonances and bandwidth is shown in Fig. 14, where N was reduced to 12. The four tested cases are all with ferrite beads applied to the turns, as documented in Table 6.

It must be noted that, although it may be possible to find a satisfactory configuration with a flat and extended enough FR, when the number of turns is reduced, the granularity increases, and small adjustments are no longer possibles as adding/subtracting one coupled turn has very appreciable difference. This is visible in Fig. 14, as each curve differs from the other by one single symmetric change. Transitions from curve 56 to 57, for example, consist of removing one turn from the bead at position 3 and 10: the consequence is an increase of bandwidth and a slight reduction of the resonance at about 15 MHz. Other attempts to further increase the bandwidth (as for curves 54 and 55) by reducing coupling cause an unsatisfactory reduction of resonance damping.

Finally a check was done of a much reduced configuration with $N = 9$ and, among others, two aspects were verified: first, FR stability was checked when input wires are moved (visible with curves all overlapped in Fig. 15) and, second, a comparison was carried out with some measurements taken by using a signal generator and a high-performance multimeter (Agilent mod. 34401A). These measurements were corrected for the high input impedance of the multimeter, introducing a 6.02 dB factor to compensate for the 50 Ω loading at the probe output of the other measurements using the VNA. It is possible to see a good agreement with maximum deviation occurring at 12 kHz and amounting to 0.58 dB.

4.2. Uncertainty estimate

4.2.1. Input impedance variability

Since the input impedance of the designed probe depends mainly on the values of the components of the RC branch, it can be easily calculated with a type B approach using the characteristics of the used components.

The number of turns had as additional minor requirement to mitigate the reduction of the flowing current resulting from the increasing inductive reactance. The resulting input impedance is thus marginally influenced by this inductive component at the largest frequency values, where with $N_2 = 12$ and the estimated 70 nH for a single turn, the resulting inductive reactance is 1900 Ω at 30 MHz.

The selected resistors are 0.1% and have a 25 ppm/°C temperature coefficient [37]. Of course better components may be used with a smaller temperature coefficient, but the low self heating leads to conclude that only the environmental temperature changes are relevant with the lowest temperatures compensated by that small amount of self heating. An excursion of 20 °C around the reference temperature of about 20 °C used for the initial calibration shows only ±500 ppm overall. The datasheet confirms a series of tests for environmental stress conditions (cold, dry heat, damp heat, vibration, bump) with maximum deviation of 0.1% that is the only prevalent term.

The capacitors C_{21} and C_{22} have some influence in the lower portion of the frequency interval, between 2 kHz and slightly beyond the cut-off frequency of 10 kHz (for the 11 nF and 1.5 kΩ combination of C_2 and R_2, respectively). Unfortunately, this type of capacitors does not receive a characterization of stability with respect to temperature and ageing. They are tested, however, for preservation of nominal value within 5% with a series of environmental stress tests (cold, dry heat, damp heat, vibration, bump) and within 10% with combined electrical stress tests (1.7 times the rated voltage, here 500 Vrms, for 1000 h), well beyond normal conditions of operation, as per IEC 60384-14 [38].

When approaching the HF portion of the interval, the contribution of the inductive reactance of the winding and the effect of the added ferrite beads becomes marginally relevant.

The uncertainty contributions to the input impedance value may be thus synthesized as:

- $e_R = 0.1\%$ for each resistor (six in series connection); since this error term is partially contributed by systematic effects, taking the uncertainty of the overall resistance R_2 as the random combination of each term may be slightly underestimating;
- $e_C = 5\%$ for each capacitor (two in series connection); also in this case the presence of some systematic error terms due to the physical behaviour of the component cannot be excluded and we assume again that the random combination may lead to a slightly underestimated uncertainty.

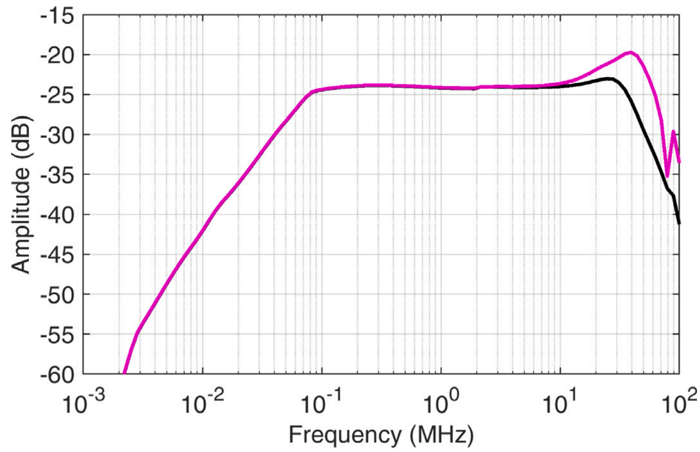

Fig. 12. Frequency response with $N = 14$: relevance of intermediate ferrite beads on selected turns (black, curve 45) compared to the case with no such ferrite beads (magenta).

Table 6
Tested cases of ferrite beads arrangements for the $N = 12$ turns coil.

Curve no.	1	2	3	4	5	6	7	8	9	10	11	12
54	N	N	N	Y1	Y2	N	N	Y2	Y1	N	N	N
55	N	Y1	Y2	Y2	N	N	N	N	Y2	Y2	Y1	N
56	N	Y1	Y1	Y2	Y2	N	N	Y2	Y2	Y1	Y1	N
57	N	Y1	N	Y2	Y2	N	N	Y2	Y2	N	Y1	N

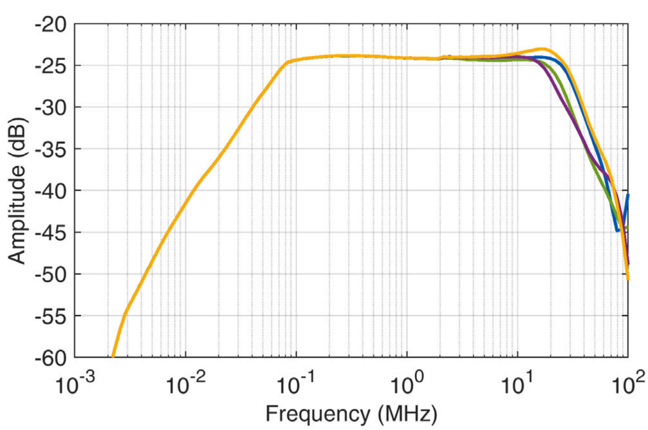

Fig. 13. Frequency response with $N = 14$: various configurations of intermediate ferrite beads on selected turns as per Table 5 (blue, curve 50; green, curve 51, purple, curve 52; yellow, curve 53). The most extended frequency response (curve 50, blue) has −24.25 dB to −24.03 dB variation, i.e. ±0.1 dB; its −3 dB frequency extension is up to 31.1 MHz.

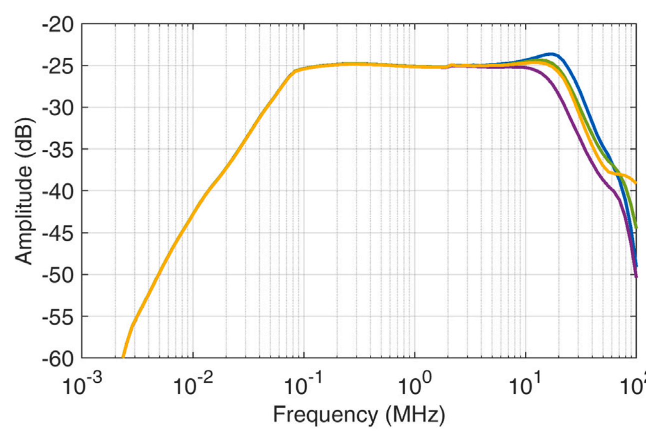

Fig. 14. Frequency response for $N = 12$ turns: various configurations of intermediate ferrite beads on selected turns as per Table 6 (blue, curve 54; green, curve 55, purple, curve 56; yellow, curve 57). The most extended frequency response (curve 57, yellow) has −25.23 dB to −24.65 dB variation, i.e. ±0.3 dB and exactly 1 dB less than curve 50 in Fig. 13; its −3 dB frequency extension is up to 24.8 MHz.

For both terms the error distribution may be assumed uniform, as such performance are meant to be guaranteed maximum deviations. The resulting uncertainty is thus:

$$u\{R_2\} = \frac{1}{\sqrt{6}}\frac{e_R}{\sqrt{3}} \qquad u\{C_2\} = \frac{1}{\sqrt{2}}\frac{e_C}{\sqrt{3}} \tag{3}$$

The formulation of the sensitivity coefficients S_R and S_C considering the fractional changes expressed by $u\{R_2\}$ and $u\{C_2\}$ is

$$S_R = \left(\frac{R_2}{|Z_{in}|}\right)^2 \qquad S_C = \left(\frac{1/(\omega C_2)}{|Z_{in}|}\right)^2 \tag{4}$$

and both are smaller than unity and equal to 0.5 at the crossover (so at the cut-off frequency of the RC circuit).

The formula of propagation

$$u\{Z_{in}\} = \sqrt{S_R^2(u\{R_2\})^2 + S_C^2(u\{C_2\})^2} \tag{5}$$

intended with coverage factor $k = 1$.

4.2.2. Frequency response variability

The FR variability is a combination of the already discussed variability terms of the passive components plus those characterizing the TBCP1 current probe. Such variability may be ascribed to ageing and variable external conditions, such as in particular temperature.

The FR may be divided into two regions: the low-frequency (LF) portion (up to some MHz), where curves for different turns arrangements are perfectly overlapped, and the HF portion, where some curve dispersion can be observed approaching the resonance with slightly different curves for various arrangements of the turns and ferrite beads.

The variability of the LF FR in the kHz and tens of kHz range is of the same kind of the variability of the input impedance discussed

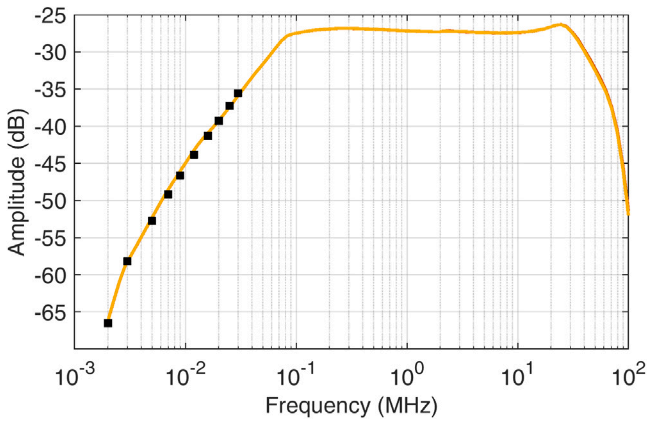

Fig. 15. Frequency response for one case with $N = 9$ turns: repeatability of connection and comparison with manually measured values (black squares).

above in Section 4.2.1), working as a voltage divider between R_2 and X_2. Then the variability of the RF current probe must be added (that is very seldom documented and may be ascribed mainly to the influence of temperature, not so much for the variation of the geometry, rather for change of the magnetic permeability of the ferrite core).

The HF FR is mainly characterized by the resonance and by its tuning using the ferrite beads, as introduced in Section 3.2.

For ferrite materials a slight influence of temperature on permeability may be assumed, usually limited to ±10% for a variation of 0 °C to 60 °C, and in line with the variability of the nominal value. We have also seen that the used ferrite beads have a reduction of inductance and increase of resistance that is not further characterized by the manufacturer and was thus studied experimentally.

Residual variability is expected instead by the geometry of the turns, i.e. touching or overlapping wires, and parasitic capacitance in general, for which the added ferrite beads are an element of normalization. For this reason, when a stable geometry is achieved after fine tuning, turns should be fixed by glue and the overall probe housing provides control of capacitive coupling with external elements. The winding geometry should then be well documented and described, in order to ensure FR repeatability for the manufactured items.

As for the uncertainty characterizing the measured FR, then, this is in direct relationship with the setup and instrumentation, as discussed in the following.

4.2.3. Frequency response setup

The experimental FR verification was carried out by using a VNA feeding an accessible 50 Ω load on port 1 (Z_L), across which the probe input terminals are connected. The port 2 is connected to the output of the current probe N connector and experiences the mismatch as declared by the manufacturer.

The VNA is used in high-power mode, sourcing a swept sine signal at 3 dBm with an IF bandwidth of 100 Hz (as a compromise between speed of measurement and noise floor). With most of the FR amounting to −40 dB to −20 dB, the corresponding S_{21} transmission magnitude uncertainty of the VNA may be assigned a value ≤ 0.06 dB with $k = 1$ as per manufacturer's datasheet [35]. The datasheet reports such values, indeed, for an IF value of 10 Hz, so that, having adopted the 100 Hz IF bandwidth value, the associated uncertainty term of 0.004 dB due to noise should be added (although it is apparent that it is not influent, being much smaller).

The presence of the probe connected in parallel at the receiving $Z_L = 50\,\Omega$ load end causes impedance mismatch, as previously observed. The resulting load impedance is $Z'_L = Z_L // Z_P \approx 48.5\,\Omega$ for $Z_P = 1.5\,\mathrm{k}\Omega$ to $1.7\,\mathrm{k}\Omega$ (accounting for various realizations, but equal to $1.5\,\mathrm{k}\Omega$ in the present case), causing a reflection coefficient $\Gamma_L = 0.015$ to 0.016. The approach was to keep the feeding cable short, shorter than $\lambda/10$ at the maximum frequency of 30 MHz to minimize the standing wave phenomenon, allowing to say that the prevailing effect is simply that of reducing the received voltage (systematic error), rather than causing variable and unknown amplitude variation with frequency.

The reflection at the other end of the line is associated to the VNA port and the manufacturer declares a better than 30 dB source match, that corresponds to a reflection coefficient $\Gamma_S = 0.032$.

The overall voltage mismatch uncertainty may be determined as

$$U = \pm \Gamma_S \Gamma_L \tag{6}$$

which ends up in ±0.051% for the present case, that is negligible.

The systematic reduction in the measured voltage at the probe input due to the loading effect can be compensated by multiplying by $1 + \Gamma_L = 1.015$, by taking the case of $Z_P = 1.5\,\mathrm{k}\Omega$. Using a single constant compensation value leads to a slight overcompensation at the lowest frequencies by effect of the additional capacitive reactance in series: in the present case with two series-connected 47 nF capacitors, the real loading effect (and consequential voltage reduction) at 5 kHz would be 0.0123, not 0.015, so with a systematic error of 0.27% if the previous compensation is applied. This compensation is not applied in the reported results.

Another potential systematic error term comes from the attenuation in the wires and coaxial cables (limited to about 0.05 dB, if the typical RG58 attenuation of 0.05 dB/m at 10 MHz is considered). This term, however, is included in the VNA calibration.

More relevant than this and not included in the calibration, there is the introduced series impedance by using the RRC ferrites to prevent CM and DM loops: such ferrites add about 80 Ω at 10 MHz on each input wire, resulting in an increased attenuation of 0.9 dB, if compared to the nominal 1500 Ω resistor.

The setup uncertainty with respect to relative movement of connections and unwanted coupling was in fact improved by inserting CM ferrites on the connecting cables (indicated by large black dots in Fig. 9), DM ferrites (effective also for CM) on the feeding wires from the BNC-4 mm adapter, and then verified by periodically measuring the transmission S_{21} with the same Through of the calibration over the entire day of tests. This resulted in a spread of curves of less than 0.2 dB up to about 20 MHz, increasing slightly beyond that.

The setup elements included in the calibration are shown in the schematic of Fig. 9 using the blue colour and those introduced for the connection of the probes are in red (with the N-BNC adapter used only for probe A in orange). It is observed that the approach is legitimate if the negligible attenuation and short electrical length of these elements are considered, valid in the range up to 30 MHz.

Finally, the uncertainty of the manual measurements taken with the multimeter is quite low. The 34401A for the range of frequencies between 10 Hz and 20 kHz (bracketing all measurements of Fig. 15 except the last two) and using the lowest scale of 100 mV has an uncertainty of 0.06%rdg + 0.04%range. As per its manual, these accuracy figures correspond to a ±4σ interval, so that a $k = 4$ coverage factor may be associated. Bringing them down to the usual $k = 2$, the corresponding uncertainty is 0.03%rdg + 0.02%range.

Readings have values comprised between 0.42 mV and about 50 mV, so that the largest uncertainty contribution occurs at 0.42 mV (the 2 kHz value) with a preponderant range contribution to the error, resulting in 8.5% with $k = 2$. The uncertainty at 5 kHz with 2.3 mVis already reduced to 1.8%. The stability of the signal generator at 10 Vpp and 20 Vpp was verified with the same 34401A when loaded with the 50 Ω termination and found better than 0.3% after a 20-minute warm-up.

Table 7
Summary of performance of the proposed Probe B (version of curve 50 with 14 turns, see Table 5) and comparison with existing voltage probes.

Performance index	Proposed Probe B	Others
Galvanic insulation	Y	N (CISPR probe) Y (IHV probe)
Attenuation	−24.1 dB	−30 dB (CISPR probe) −40 dB (IHV probe)
Flatness of frequency response	±0.1 dB	±1 dB to 1.5 dB (CISPR probe) several dB (IHV probe)
Frequency extension	31.1 MHz	30 MHz to 70 MHz for CISPR and IHV probes
Output noise bandwidth 30 MHz	4.9 μV (50 Ω ref.)	similar (CISPR probe) ≥ 0.9 mV (IHV probe)
Common-mode influence	N	N (CISPR probe) Y (IHV probe)
Approximate price[a]	≈370 EUR	≈700–2000 EUR

[a] Price of probe B estimated from 330 EUR for TBCP1-200 and 40 EUR for passives, enclosure and connectors.

5. Conclusion

The proposed voltage probe B exploits the measurement of the current flowing through a known impedance branch by using a commercial RF current probe. In this way it achieves galvanic insulation and low noise (that of the RF current probe, corresponding approximately to a 50 Ω resistor, as it is for many RF probes, including the CISPR voltage probe).

The minimum input impedance recommended by CISPR is achieved by selecting a 1500 Ω input resistor and the consequential reduction of the current is compensated by applying N_2 turns through the RF current probe (the preferred configuration is with $N_2 = 14$ (curve 50) showing a smaller attenuation and an extended frequency response up to 30 MHz). This arrangement is not exempt from stray inductance due to the N-turn coil on the probe ferrite material. An estimate of 60 nH/turn, assuming an average HF relative permeability of 100, was used during the design that turned out to be reliable with the experimental verification.

Such composite voltage probe resulted in an attenuation of only about 24 dB in the centre band, so with a performance improved by about 6 dB over the CISPR probe (that does not have galvanic insulation either) and by 16 dB over the simpler solution (indicated as "Probe A"), using the insulated high-voltage probe (that does not have sufficient fundamental attenuation and much higher noise).

The attenuation of the fundamental (assumed 50 Hz) and its harmonics is of some relevance in order to optimize resolution and sensitivity of the connected instrumentation, avoiding large signal excursion at LF that would require too a large dynamic range. Thanks to the combined effect of the RC input branch and the desensitization of the RF current probe towards LF, the achieved 50 Hz suppression is more than three orders of magnitude at 80 dB, enough to bring the fundamental amplitude down to the tens of mV range.

The side effect of the N-turn winding is the introduction of a HF resonance, for which small ferrite beads inserted between selected turns were used, introducing secondary magnetic coupling with additional losses between non-adjacent turns (this arrangement resembles that of cross-coupled filters). This control measure is effective if it can be precisely trimmed with inductive coupling terms of the same amount of the inductance of one turn. When the number of turns is too low, trimming granularity appears and the frequency response cannot be shaped as desired down to a fraction of dB of amplitude, ensuring the necessary few MHz of frequency extension. Smaller ferrites should be considered to this aim, although an excessive reduction of the number of turns is not of interest, having a target centre-band attenuation of −22 dB and a frequency extension of 30 MHz. In addition, the used ferrite beads were selected with a trade-off between the applied inductance and introduced resistive term, with an extensive experimental verification for many geometries.

A consolidated version with 14 turns and coupling between turns at 2/5 and 3/5 of the coil length is considered as the definitive one (curve 50 of the reported results), with very flat frequency response (within ±0.1 dB) at −24.1 dB of centre gain and extended up to 31 MHz, intended as the −3 dB point. Frequency dependent systematic error terms amounting to about 1 dB overall to add to the measured attenuation.

It is acknowledged that the proposed architecture has an intrinsic limit due to the trade-off between sensitivity and number of turns through the RF current probe, that limit the frequency response at high frequency, in particular introducing a resonant behaviour. The insertion of ferrite beads controls such resonance at the expense of limiting the frequency extension. Higher sensitivity is not achievable by increasing the number of turns, as well as further frequency extension without giving up some sensitivity.

The performance discussed above are synthesized in Table 7 for clarity and quick reference.

The designed and tested voltage probe finds its application in low-voltage grids (both DC and AC) for the measurement of conducted emissions and distortion, more safely than using a non-insulated CISPR probe and with better performances in terms of attenuation and noise than commercial insulated high-voltage probes.

CRediT authorship contribution statement

Andrea Mariscotti: Writing – review & editing, Writing – original draft, Validation, Methodology, Investigation, Funding acquisition, Conceptualization.

Declaration of competing interest

The authors declare the following financial interests/personal relationships which may be considered as potential competing interests: Andrea Mariscotti reports financial support was provided by EURAMET European Metrology Programme for Innovation and Research. If there are other authors, they declare that they have no known competing financial interests or personal relationships that could have appeared to influence the work reported in this paper.

Acknowledgements

This work was supported in part by the European Metrology Programme for Innovation and Research (EMPIR), Germany, co-funded by the European Union's Horizon 2020 research and innovation programme and the EMPIR participating states, under the Project 23IND06 "Met4EVCS".

Data availability

No data was used for the research described in the article.

References

[1] J. Pinto, B. Grasel, J. Baptista, Analysis of supraharmonics emission in power grids: A case study of photovoltaic inverters, Electronics 13 (24) (2024) 4880, http://dx.doi.org/10.3390/electronics13244880.

[2] M. Sigle, W. Liu, K.D. Karlsruhe, On the impedance of the low-voltage distribution grid at frequencies up to 500 kHz, in: IEEE International Symposium on Power Line Communications and Its Applications, IEEE, 2012, pp. 30–34, http://dx.doi.org/10.1109/isplc.2012.6201340.

[3] I. Fernandez, M. Alberro, J. Montalban, A. Arrinda, I. Angulo, D. de la Vega, A new voltage probe with improved performance at the 10 kHz – 500 kHz frequency range for field measurements in LV networks, Measurement 145 (2019) 519–524, http://dx.doi.org/10.1016/j.measurement.2019.05.106.

[4] S. Büyük, A. Mariscotti, K. Štibernik, O. Şen, M. Wojciechowski, A portable VNA-based system for grid impedance measurements, in: 2024 International Symposium on Electromagnetic Compatibility – EMC Europe, IEEE, 2024, pp. 464–469, http://dx.doi.org/10.1109/emceurope59828.2024.10722179.

[5] P. Nuutinen, A. Pinomaa, P. Peltoniemi, T. Kaipia, J. Karppanen, P. Silventoinen, Common-mode and RF EMI in a low-voltage DC distribution network with a PWM grid-tie rectifying converter, IEEE Trans. Smart Grid 8 (1) (2017) 400–408, http://dx.doi.org/10.1109/tsg.2016.2602845.

[6] CISPR 11, Industrial, Scientific and Medical Equipment — Disturbance Characteristics — Limits and Methods of Measurement, IEC, Geneva, Switzerland, 2015.

[7] A. Mariscotti, A. Mingotti, The effects of supraharmonic distortion in MV and LV AC grids, Sensors 24 (8) (2024) 2465, http://dx.doi.org/10.3390/s24082465.

[8] IEEE Std. 1688, IEEE standard requirements for the control of electromagnetic interference characteristics of replaceable electronic modules, 2015.

[9] M. Agazar, G. D'Avanzo, G. Frigo, D. Giordano, C. Iodice, P.S. Letizia, M. Luiso, A. Mariscotti, A. Mingotti, F. Munoz, D. Palladini, G. Rietveld, H. van den Brom, Power grids and instrument transformers up to 150 kHz: A review of literature and standards, Sensors 24 (13) (2024) 4148, http://dx.doi.org/10.3390/s24134148.

[10] CISPR 16-1-2, Specification for Radio Disturbance and Immunity Measuring Apparatus and Methods — Part 1-2: Radio Disturbance and Immunity Measuring Apparatus – Coupling Devices for Conducted Disturbance Measurements, CISPR, 2017, IEC, Geneva, Switzerland.

[11] IEC 61869-1, Instrument Transformers — General Requirements for Instrument Transformers, IEC, Geneva, Switzwerland, 2023.

[12] M. Tefferi, N. Nakamura, B. Barnes, N. Uzelac, Supraharmonic measurements in distributed energy resources – Power quality observations in a microgrid, 2022, https://powerside.com/supraharmonic-measurements-in-distributed-energy-resources-power-quality-observations-in-a-microgrid/.

[13] S. Xie, Z. Mu, W. Ding, Z. Wan, S. Su, C. Zhang, Y. Zhang, Y. Xia, D. Luo, Development of broadband resistive–capacitive parallel–connection voltage divider for transient voltage monitoring, Energies 15 (2) (2022) 451, http://dx.doi.org/10.3390/en15020451.

[14] CISPR 16-2-1, Specification for Radio Disturbance and Immunity Measuring Apparatus and Methods — Part 2-1: Methods Of Measurement of Disturbances and Immunity – Conducted Disturbance Measurements, CISPR, 2017, IEC, Geneva, Switzerland.

[15] S. Lodetti, J. Bruna, J.F. Sanz, J.J. Melero, Characterization of the emission of an electric bus inductive charging in the 2 kHz to 150 kHz range, in: AEIT International Conference of Electrical and Electronic Technologies for Automotive, AEIT AUTOMOTIVE, IEEE, 2019, pp. 1–6, http://dx.doi.org/10.23919/eeta.2019.8804604.

[16] T.M.H. Slangen, T. van Wijk, V. Cuk, J.F.G. Cobben, The harmonic and supraharmonic emission of battery electric vehicles in The Netherlands, in: International Conference on Smart Energy Systems and Technologies, SEST, IEEE, Istanbul, Turkey, 2020, pp. 1–6, http://dx.doi.org/10.1109/sest48500.2020.9203533.

[17] A. Delle Femine, D. Gallo, C. Landi, M. Luiso, H.E. van den Brom, R. van Leeuwen, Assessment of quasi-stationary power quality phenomena in DC power systems, Measurement 242 (2025) 115844, http://dx.doi.org/10.1016/j.measurement.2024.115844.

[18] Hameg, HZ probes datasheet, 2024, https://www.tequipment.net/Hameg/HZ115/. (available online, last access on 13 May 2025).

[19] Tektronix, THDP0100/0200 and TMDP0200 –high voltage differential probes, 2015, 077-0540-01.

[20] Testec, SI-9002 differential voltage probe, 2016.

[21] Testec, SI-9010 differential voltage probe, 2016.

[22] Hioki, Differential probe 9322 – manual, 2021, https://www.hioki.com/euro-en/products/data-acquisition/recorder-options/id_5945.

[23] I. Fernández, A. Gallarreta, J. González-Ramos, P. Wright, D. de la Vega, I. Angulo, A. Arrinda, Measurement system of the mean and sub-cycle LV grid access impedance from 20 kHz to 10 MHz, IEEE Trans. Power Deliv. 38 (3) (2023) 2204–2212, http://dx.doi.org/10.1109/tpwrd.2023.3238647.

[24] C. Carobbi, L. Millanta, Circuit loading in radio-frequency current measurements: The insertion impedance of the transformer probes, IEEE Trans. Instrum. Meas. 59 (1) (2010) 200–204, http://dx.doi.org/10.1109/tim.2009.2022450.

[25] IEC 61010-1, Safety Requirements for Electrical Equipment for Measurement, Control, and Laboratory Use — Part 1: General Requirements, IEC, Geneva, Switzerland, 2016.

[26] EN 61000-4-5, Electromagnetic Compatibility (EMC) — Part 4-5: Testing and Measurement Techniques – Surge Immunity Test, CENELEC, Brussels, Belgium, 2017.

[27] EN 140401-801, Detail specification: Fixed low power film SMD resistors — Rectangular — Stability classes 0,1; 0,25; 0,5; 1, 2013.

[28] CISPR 15, Electromagnetic Compatibility (EMC) — Limits and Methods of Measurement of Radio Disturbance Characteristics of Electrical Lighting and Similar Equipment, IEC, 2018, IEC, Geneva, Switzerland.

[29] IEC 61000-4-30, Electromagnetic Compatibility (EMC) — Part 4-30: Testing and Measurement Techniques – Power Quality Measurement Methods, IEC, 2015, IEC, Geneva, Switzerland.

[30] TekBox Digital Solutions, TBCP1 25 mm fixed aperture RF current monitoring probes (TBCP1-200), 2024, https://www.tekbox.com/product/TBCP1_200_Manual.pdf.

[31] Richco, RT toroid cores, 2006, https://www.tme.eu/en/details/rt-80-60-50/ring-ferrites/richco/. (available online, last accessed on 14 June 2025).

[32] K.-H. Um, Derivation of transfer function for the cross-coupled filter systems using chain matrices, Int. J. Adv. Smart Converg. 7 (1) (2018) 7–14, http://dx.doi.org/10.7236/IJASC.2018.7.1.2.

[33] D. Zaikin, Model of the Rohde & Schwarz EZ-17 Current Probe and Creation of a DIY Analog for EMI Study, Institute of Electrical and Electronics Engineers (IEEE), 2022, http://dx.doi.org/10.36227/techrxiv.19199660.v1, TechRxiv.

[34] Agilent, 34401A 6 1/2 Digit Multimeter, eighth ed., 2012, 34401-90004.

[35] Anritsu MS2036C, Technical datasheet, 11410-00548, rev. AW, 2024, https://dl.cdn-anritsu.com/en-us/test-measurement/files/Brochures-Datasheets-Catalogs/datasheet/11410-00548AW.pdf.

[36] Richco, RRC split ferrite cores with plastic casing, 2010, https://www.tme.eu/en/details/rrc-16-8-16-m/ferrites-for-cables/richco/. (available online, last accessed on 14 June 2025).

[37] Viking, Thin film precision chip resistor – AR series, 2024, https://www.viking.com.tw/en/category/Resistor-ARBTC.html.

[38] IEC 60384-14, Fixed capacitors for use in electronic equipment — Part 14: Sectional specification – Fixed capacitors for electromagnetic interference suppression and connection to the supply mains, 2016.